Polymeric optofluidic Fabry–Perot sensor by direct laser machining and hot embossing

Jing Wu,[1,2] Daniel Day,[1,*] and Min Gu[1]

[1]Centre for Micro-Photonics, Faculty of Engineering and Industrial Sciences, Swinburne University of Technology, Hawthorn, PO Box 218, Victoria 3122, Australia

[2]Institute of Advanced Nanophotonics, State Key Laboratory of Modern Optical Instrumentation, Zhejiang University, Hangzhou 310027, China

*Corresponding author: dday@swin.edu.au

Received 19 November 2010; revised 3 March 2011; accepted 4 March 2011; posted 8 March 2011 (Doc. ID 138467); published 25 April 2011

We present a polymeric-based Fabry–Perot optofluidic sensor fabricated by combining direct laser machining and hot embossing. This technique provides a more elegant solution to conventional hot embossing by increasing the production rate, improving the reproducibility, and further reducing the cost, providing a large working area and flexibility in design modification and customization. As a proof of concept, a Fabry–Perot (F–P) optofluidic sensor was fabricated in polymethyl methacrylate (PMMA) from a micromachined stamp. The experimental results of the sensor agree well with analytical calculations and show a sensitivity of 2.13×10^{-3} RIU/nm for fluid refractive index change.

OCIS codes: 230.4000, 220.4610, 120.2230, 130.6010, 280.4788.

1. Introduction

In the development of microfluidic technology toward biomedical and clinical applications, disposable microfluidics has generated a lot of interest for the purpose of reducing possible cross contamination and misdiagnosis. These devices usually require low cost of fabrication, high volume production, good reproducibility, and versatility in design for a wide spectrum of applications. As polymer materials have became more prevalent as cost-efficient alternatives to glass, more polymer-based techniques (such as hot embossing [1] and microinjection molding [2]) have been employed in the past decade more than the conventional glass-based micro-electro-mechanical-systems (MEMS) techniques. Among these techniques, hot embossing is typically used when high precision and quality are needed and is a simple and economical process with high scalability and good repeatability. Considering the investment and fabrication cost, conventional photolithography is usually preferred to laser-based lithography techniques for the master stamp fabrication in hot embossing. The downsides include the requirements for a multistep process and chemical posttreatment, which also affect the production rate. Another disadvantage is the short life cycle of the master during the embossing process, which is, in some cases less than five times [3]. More importantly, both photolithography and laser-based lithography lack the flexibility in design modification. For applications such as DNA sequencing or point-of-care diagnostics, the microdevices also require comparably large surface areas or long reaction length for high-throughput data collection to ensure accurate diagnosis. As a result, the ideal fabrication method should have the ability to deal with large surface areas and be flexible to enable design modifications.

In this paper we present a new method of cost-efficient and convenient fabrication of a polymeric-based microfluidic optical sensor by combining direct laser machining and hot embossing. The application of lasers has been proven to be important in MEMS

0003-6935/11/131843-07$15.00/0

both in system operations like particle manipulation [4–6] and sensing [7–9] or microdevice fabrication [10–14]. In our experiment, the fast, single step, automated process of laser machining provides an appealing solution to several major disadvantages of conventional hot embossing by increasing the production rate, improving the reproducibility, reducing the cost, enabling a robust stamp with longer life, providing large working areas and flexibility in design modification and customization. A proof of concept F–P sensor was integrated with a microfluidic channel in PMMA for optofluidic sensing.

2. Experiment

A. Device Design

As shown in Fig. 1 (the insets), a microfluidic device with an F–P cavity incorporated within the microchannel (shown as the square regions in the middle of the straight microchannel) was produced. The top layer had holes drilled at the inlet and outlet for connectors. The fluid was pumped into the microchannel, which filled the F–P cavity; the refractive index was characterized by the transmission signal through the F–P cavity. PMMA was selected as the sensor substrate for several reasons in addition to the low cost advantage of the polymer material. The commercial availability and fabrication simplicity (low transition temperature) and biological compatibility make it ideal for laboratorial/industrial mass production.

B. Device Fabrication

The device was fabricated by four steps as illustrated in Fig. 2. First, a 10∶1 ratio of the poly(dimethyl siloxane) (PDMS) prepolymer and its curing agent (Sylgard 184, Dow Corning) were mixed and spin-coated at a speed of 1500 RPM onto a silicon wafer (Cemat Silicon S. A.). The wafer was then placed on a hotplate and heated at 75 °C for 20 min. When the PDMS was cured, the master stamp of the channel structure was cut out of the PDMS layer by a CO_2 laser (Universal Laser Systems). The automated laser cutting process takes a few minutes and was controlled by a computer. After the cutting process, the PDMS residue was peeled off from the wafer, leaving an inverse pattern of the designed microfluidic device (the master stamp). The wafer was cleaned in distilled water in an ultrasonic bath for 10 min, followed by several methanol rinses in order to remove any residue.

In the second step, a manual embossing system was placed onto a hotplate and was preheated to 150 °C for 1 h to reach a uniform temperature. A layer of PMMA was sandwiched between the master stamp and a piece of glass and inserted into the embossing system. The purpose of the additional glass layer is to ensure a smooth molding surface when removing the whole structure from the embossing system. The embossing system comprises two water-cooled platens that are preheated while in contact via a hotplate. A calibrated torque wrench is used to apply pressure on the stamp and substrate that are placed between the two platens, by tightening a screw that presses the top platen against the bottom platen. The pattern on the master stamp was embossed in the PMMA substrate under a pressure created by 10 Nm torque from a torque wrench, at a temperature of 150 °C for 10 to 15 min, before being cooled down to room temperature by circulating water for 5 min. Once cooled, the sample was removed from the embossing system and the PMMA substrate was carefully peeled from the master stamp.

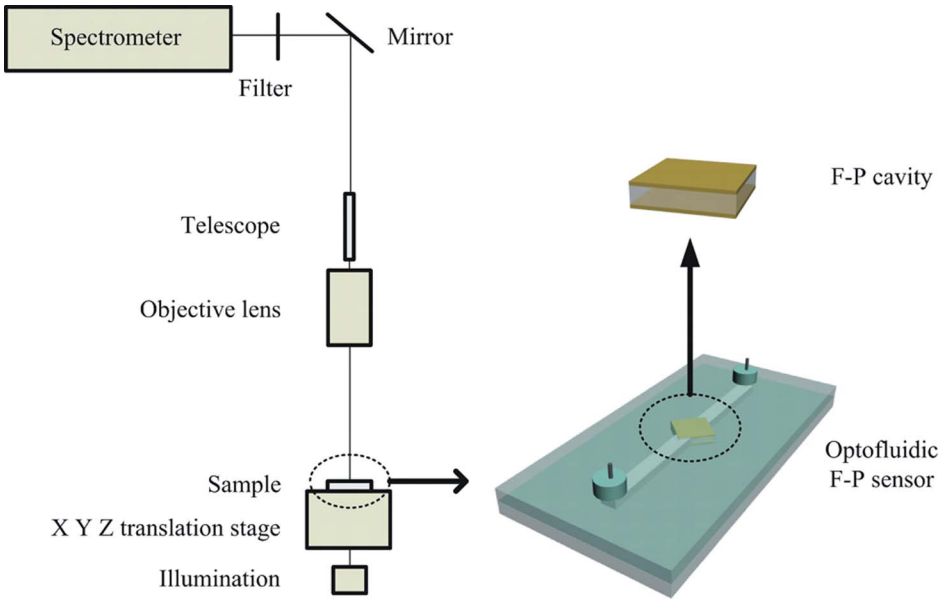

Fig. 1. (Color online) Schematic illustration of the experimental system. The insets show the details of the optofluidic sensor that was made up of an F–P cavity (demonstrated in the enlarged top inset) integrated within a PMMA microfluidic channel.

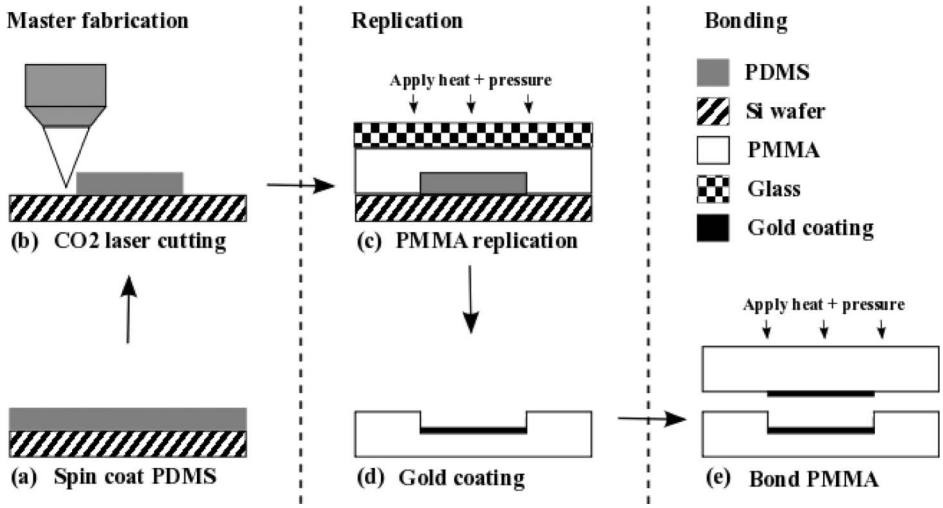

Fig. 2. Fabrication procedure for the F–P optofluidic sensor. (a) Spin coating of a PDMS layer onto a silicon wafer, (b) CO_2 laser cutting of the device template and removal of the unwanted PDMS, (c) embossing of the PDMS template into a PMMA substrate creating the master stamp, (d) gold coating of the sensing region using a shadow mask, and (e) alignment and bonding of the optofluidic sensor.

In the third step, in order to improve the cavity quality and to explore for potential sensitivity enhancement, the channel surface in the F–P cavity is coated with thin gold film. The PMMA substrate was put under a shadow mask to coat a gold layer onto the sensing region in the microchannel. Another blank piece of PMMA was also coated with gold to the same thickness using the shadow mask. Finally, holes were drilled by the CO_2 laser at the inlet and outlet positions.

In the forth step, the two pieces of PMMA were aligned manually under an inspection microscope with 4× magnification to achieve a precision within a few tens of micrometers, and a drop of superglue was placed on each of the four edges to hold the pieces in place during the bonding. The aligned PMMA layers were then placed into the embossing system under 10 Nm pressure at a temperature of 75 °C for 30 min for thermal bonding. Connectors were then glued to the inlet and outlet openings on the device and connected to a syringe pump via silicon tubing.

3. Result and Discussion

A. Fabry–Perot Sensing Mechanism

The Fabry–Perot cavity, also referred to as a Fabry–Perot interferometer or an etalon, shown in Fig. 3(a), consists of two parallel flat partially transparent mirrors (two gold coated PMMA surfaces) separated by a fixed distance with an optical-transparent bulk material in between them. The broadband light incident upon it undergoes multiple reflections between the mirrors, resulting in transmission peaks in the output spectrum, which correspond to resonances of the F–P cavity [shown in Fig. 3(a) inset]. The wavelengths of the peaks are determined by the condition

$$nd = \frac{m\lambda}{2}, \qquad (m = 1, 2, 3, \ldots), \tag{1}$$

where d is the distance between two reflective surfaces, n is the refractive index of the bulk material in between the mirrors, and λ is the wavelength of the light in a vacuum. In our experiment, the fluid channel runs through the F–P cavity and fills the cavity with fluid of different refractive indices. The resonance peaks from the F–P cavity are shifted by the refractive index of the fluid inside the channel. By monitoring the shift of the F–P resonance peaks on a spectrometer, the fluid refractive index can be determined.

B. System Optimization and Calibration

After devices with different thickness of gold coating (20 and 40 nm) were fabricated, they were mounted onto a translation stage and characterized by a spectrometer (the experimental system as shown in Fig. 1). The spectral resolution of the spectrometer in the experiment was 0.2 nm. Objective lenses of different numerical apertures (NA) were used to optimize the system. The transmission spectra from the F–P cavities were measured with no liquid inside the microfluidic channels. The F–P resonance peaks were observed using 0.24, 0.5, and 0.70 NA objective lenses for both samples. Figure 4 shows the calculated finesse (a) and visibility (b) of the cavities from the spectral results. Equations (1) and (2) are the equations for finesse and visibility calculations. Comparison between the two figures demonstrates that the 20 and 40 nm samples have higher transmissivity but lower visibility with lower NA lenses. The lower NA lenses have higher transmission efficiency across the broad wavelength range used in the illumination light resulting in the higher transmission signal for the F–P resonances. Taking into consideration the finesse and visibility, a higher resolution F–P signal could be collected when using the higher

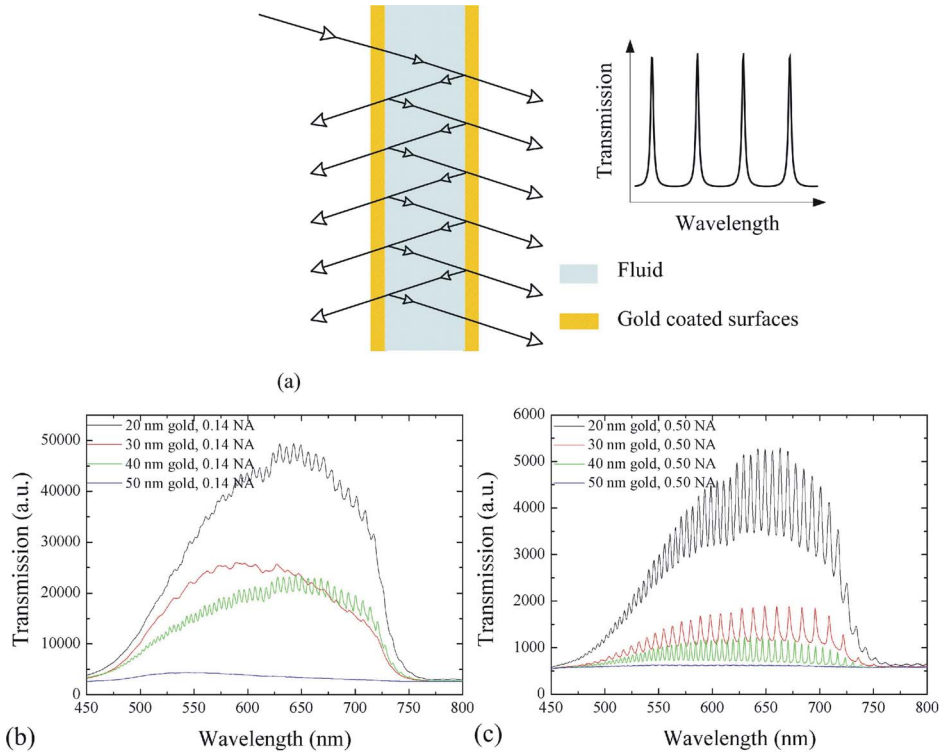

Fig. 3. (Color online) (a) Schematic illustration of the principle of an F–P cavity. The output spectrum of the transmission signal shows a series of peaks with respect to different wavelengths. (b) The transmission spectra of the samples with different gold coating thickness (20, 30, 30, and 40 nm) using objective lenses of (b) NA = 0.14 and (c) NA = 0.5.

NA lenses. The higher NA objective lenses enable the capture of higher spatial frequencies transmitted through the F–P, which could result from diffuse reflections in the sensor caused by: (1) the increased surface roughness of the PMMA/gold surface compared with high quality mirrors, (2) debris/contamination in the sensor from the fabrication process, or (3) low quality and nonuniform thickness gold coating resulting in pinholing. The finesse and visibility of the 40 nm sample were higher than the 20 nm sample with all the objective lenses used.

Measurements with the 0.5 NA objective lens have shown better finesse and visibility compared to lower NA cases [presented in Figs. 3(b) and 3(c)], while there was a slight drop in the visibility in the measurements with the 0.7 NA objective lens. In the following experiments, the 0.5 NA objective lens was chosen to work with the optofluidic devices for refractive index detection. The finesse, F, of the resonant cavity is given by

$$F = \frac{\lambda^2}{2nd\delta\lambda}, \tag{2}$$

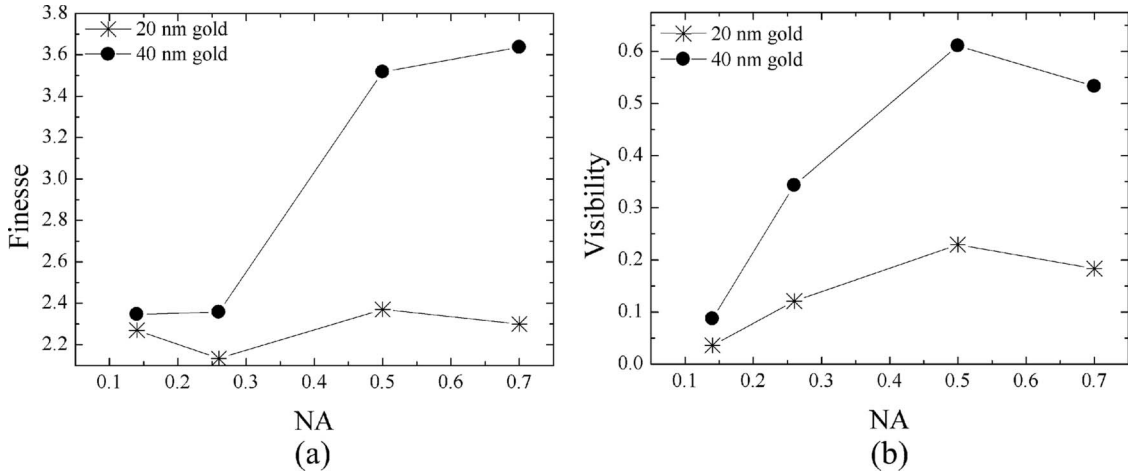

Fig. 4. Finesse (a) and visibility (b) calculated from the spectra collected with different NA objective lenses of the sensors with 20 and 40 nm gold coating.

where $\delta\lambda$ is the FWHM of the resonant peak. The visibility, V, of the resonant cavity is

$$V = \frac{I_{\max} - I_{\min}}{I_{\max} + I_{\min}}, \tag{3}$$

where $I_{\max}$ and $I_{\min}$ are the maximum and minimum intensities of the resonances in the transmission spectra.

The optofluidic sensor with 20 nm gold coating was selected to be theoretically studied and experimentally tested for the fabrication calibration. The experimental transmission signal from a device of 20 nm gold coating was compared with theoretical calculated spectra (normalized). As shown in Fig. 5(a), for both theoretical and experimental results, there exist five peaks from 625 to 660 nm wavelength range. The distance between adjacent peaks is about 6.5 nm. As shown in the figure, the variation between theoretical peaks to experimental peaks is within 2 nm within the measured wavelength range, with both peaks almost overlapped with each other at around 650 nm. The experiment result agrees well with the theoretical calculation for the microfluidic device with 20 nm gold coating; however, discrepancies between the "idealistic" theoretical case and the experimentally measured F–P data are likely to result from any of the following: (1) reduced quality or nonuniform thickness of the gold coated surfaces resulting a difference between the actual and theoretical values for reflection, transmission, and absorption of the gold layer; (2) atmospheric disturbances, such as pressure, temperature, and/or humidity; and (3) the temperature dependence of the properties of the PMMA substrate and/or gold layer as a result of heating due to the illumination light.

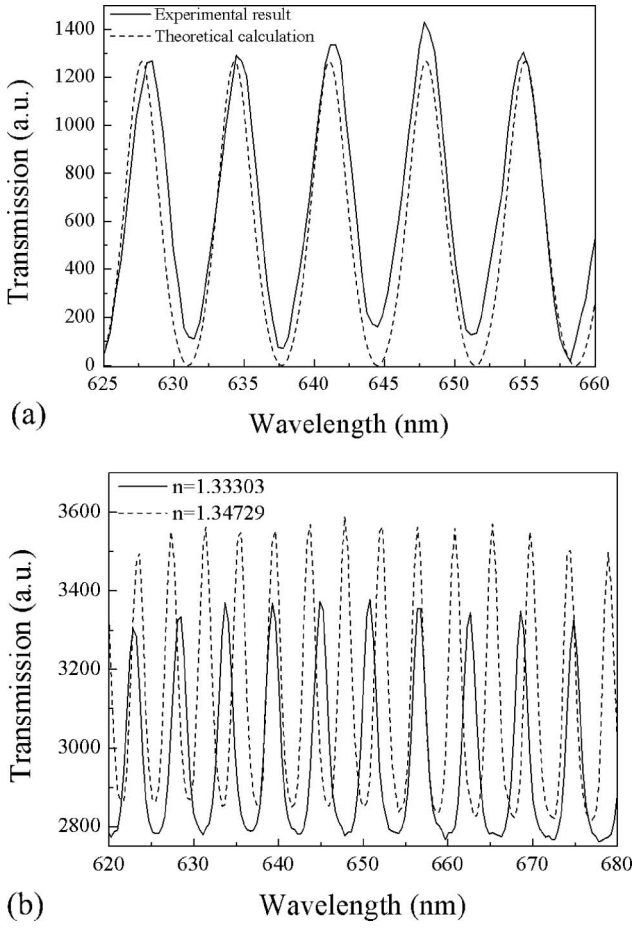

Fig. 5. (a) Experimental and theoretical calculation of the device with the 20 nm gold coating. (b) Measured transmission spectra of the 40 nm gold coated device using fluids of two different refractive indices ($n = 1.33303$ and 1.34729).

C. Fabry–Perot Optofluidic Sensing

After sensor fabrication and calibration, detection of fluid refractive index was demonstrated by the optofluidic sensor. Fluids of different refractive indices ranging from 1.33303 up to 1.43087 were made from glycerine-water solutions of different concentrations (as shown in Table 1) based on the technical instructions for OPTIM glycerine from Dow Chemical Company [15]. The refractive index of the glycerine-water solutions was confirmed via comparison with calibrated refractive index oils (Cargille Labs) using a refractometer. Devices containing F–P cavities with 20 and 40 nm gold coating were used in the measurements. The solutions of different refractive indices were spectroscopically characterized by their transmission signal through the F–P cavities in the microchannels. A basement measurement was taken beforehand with the empty microchannels ($n = 1$) before any solution was pumped into the microchannels. Between each measurement the microchannels were rinsed with deionised water. Figure 5(b) shows an example of the modulation of refractive index over the resonance shifts. The two arrows indicate that the corresponding F–P resonance peak was shifted by the refractive index change. When the fluid refractive index increases from 1.33303 to 1.34729, the F–P resonance peak shifted toward longer wavelengths, from 645 to 652 nm in the transmission spectra.

Figure 6 presents the position of the F–P resonance peak positions from spectroscopic measurements determined by the fluid refractive indices. The positions of the F–P resonance peaks shift toward longer wavelengths as the refractive index of the fluid is increased (from 1.33303 to 1.43087).

Table 1. Refractive Index of Glycerine-Water Solutions (20 °C)

Glycerine (w%)	Refractive Index
72	1.43087
63	1.41746
53	1.40256
44	1.38953
33	1.37472
23	1.36141
12	1.34729
0	1.33303

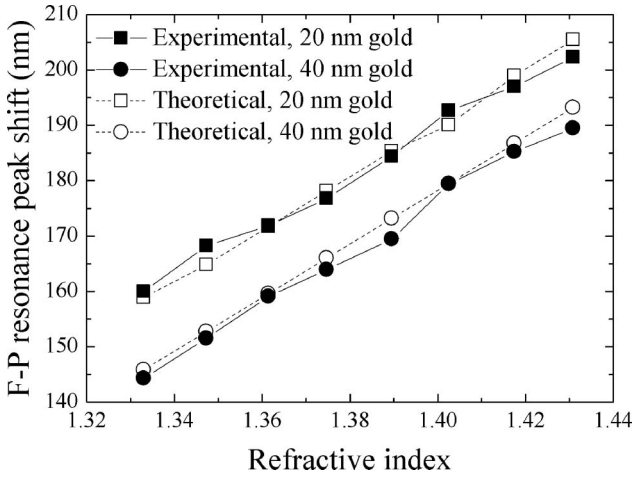

Fig. 6. Measured F–P resonant peak positions for two samples (with 20 and 40 nm gold coatings) using glycerine-water solutions of different refractive indices.

The positions of the F–P resonances were recorded and plotted as a function of the refractive index. It is observed that the resonance peak shift has a linear relationship to the fluid refractive index in the microchannel. Different results were observed by the devices of 20 and 40 nm thicknesses of gold coatings. The explanation relies on the phase change of light by metal absorption. In a simple F–P model, usually the mirrors are assumed to be perfect (highly reflected and no absorption). But in real case, the metal films coated on the mirror surfaces DO absorb and cause phase changes to the light propagating in the F–P cavity, thus, a variation in the film thickness would have an impact on the sensing result based on interferometry. Additionally, as the mechanical and optical properties of the polymer and gold coatings are temperature dependent, variations in the spectral measurements could occur. To reduce the temperature effect the devices are mounted onto a thick metal plate on the translation stage that acts as a heat reservoir.

The sensor sensitivity is defined as the detectable change in fluid refractive index as a function of the F–P resonance shift ($\Delta n/\Delta\lambda$) in the spectroscopic measurements. In our experiments, a sensitivity of 469 nm/RIU is achieved using the optofluidic sensor with the 20 nm gold coating. This sensitivity enables the limit of detection of a change in the refractive index of 2.13×10^{-3} per 1 nm shift in the F–P resonance spectrum. As the FWHM of the resonance peaks is of the order of 2.5 nm, a 1 nm shift is easily detectable. The minimum detectable wavelength change is dependent on the resolution of the spectrometer and the finesse of the cavity. By improving the resolving power of the spectrometer or increasing the quality of the F–P, the resolution could be further improved. During typical biological or chemical sensing, the anticipated shift in the resonance spectrum is likely to be less than the peak-to-peak distance of the resonances, which is approximately 10 nm. However, should the shift become larger than 2π, there is the possibility that ambiguities in the measurement may occur. To address this, the device could be modified to incorporate a multicavity F–P or simultaneous measurement of a separate reference cavity.

4. Conclusion

In summary, a new method has been presented that integrates a microfluidic device and an optofluidic sensor by combining direct laser machining and hot embossing processes. A gold coated F–P optofluidic sensor was fabricated in PMMA for fluid refractive index detection. The experimental performance of the sensor was confirmed by theoretical calculation, and a sensitivity of 469 nm/RIU was achieved, which equates to a limit of detection of 2.13×10^{-3} RIU. This technique ensures the fabrication of hot embossing masters at an increased production rate, with a better flexibility in design modification and a potentially large surface area patterning ability. It is suitable for the research and development of disposable microfluidic chips and holds great potential of commercialization with efficient high-volume production. This fabrication technique can be applied to the production of more complex two-dimensional patterns, rather than the single microchannel demonstrated in this paper, such as the fabrication of straight or curved multichannel devices. There is also the possibility of producing three-dimensional devices based on layering of the replicated PDMS layers from different PMMA master stamps. With further refinements, this technique could extend to the integration of optical, electrical, and fluidic components to various polymer microplatforms.

The authors would like to acknowledge Swinburne University of Technology through the Swinburne University Postgraduate Award and the Cooperative Research Centre for Polymers. Zhejiang University is J. Wu's current address and the work in this paper was fully completed at Swinburne University of Technology.

References

1. H. Becker and U. Heim, "Hot embossing as a method for the fabrication of polymer high aspect ratio structures," Sens. Actuators A, Phys. **83**, 130–135 (2000).
2. R.-D. Chien, "Micromolding of biochip devices designed with microchannels," Sens. Actuators A, Phys. **128**, 238–247 (2006).
3. M. B. Esch, S. Kapur, G. Irizarry, and V. Genova, "Influence of master fabrication techniques on the characteristics of embossed microfluidic channels," Lab Chip **3**, 121–127 (2003).
4. M. P. MacDonald, G. C. Spalding, and K. Dholakia, "Microfluidic sorting in an optical lattice," Nature **426**, 421–424 (2003).
5. J. Enger, M. Goksor, K. Ramser, P. Hagberg, and D. Hanstorp, "Optical tweezers applied to a microfluidic system," Lab Chip **4**, 196–220 (2004).
6. M. Ozkan, M. Wang, C. Ozkan, R. Flynn, and S. Esener, "Optical manipulation of objects and biological cells in microfluidic devices," Biomed. Microdevices **5**, 61–67 (2003).
7. E. Eriksson, J. Scrimgeour, J. Enger, and M. Goksor, "Holographic optical tweezers combined with a microfluidic device

for exposing cells to fast environmental changes," Proc. SPIE **6592**, 65920P (2007).
8. H. Mushfique, J. Leach, H. Yin, R. Leonardo, M. Padgett, and J. Cooper, "3D mapping of microfluidic flow in laboratory-on-a-chip structures using optical tweezers," Anal. Chem. **80**, 4237–4240 (2008).
9. J. Wu, D. Day, and M. Gu, "Shear stress mapping in microfluidic devices by optical tweezers," Opt. Express **18**, 7611–7616 (2010).
10. A. Marcinkevičius, S. Juodkazis, M. Watanabe, M. Miwa, S. Matsuo, H. Misawa, and J. Nishii, "Femtosecond laser-assisted three-dimensional microfabrication in silica," Opt. Lett. **26**, 277–279 (2001).
11. Y. Cheng, K. Sugioka, and K. Midorikawa, "Microfluidic laser embedded in glass by three-dimensional femtosecond laser microprocessing," Opt. Lett. **29**, 2007–2009 (2004).
12. Y. Cheng, K. Sugioka, K. Midorikawa, M. Masuda, K. Toyoda, M. Kawachi, and K. Shihoyama, "Three-dimensional micro-optical components embedded in photosensitive glass by a femtosecond laser," Opt. Lett. **28**, 1144–1146 (2003).
13. F. He, Y. Cheng, L.-L. Qiao, C. Wang, Z.-Z. Xu, K. Sugioka, and K. Midorikawa, "Two-photon fluorescence excitation with a microlens fabricated on the fused silica chip by femtosecond laser micromachining," Appl. Phys. Lett. **96**, 041108 (2010).
14. J. Wu, D. Day, and M. Gu, "A microfluidic refractive index sensor based on an integrated three-dimensional photonic crystal," Appl. Phys. Lett. **92**, 071108 (2008).
15. *OPTIM™ Glycerine* (Dow Chemical Company, 2011), retrieved http://msdssearch.dow.com/PublishedLiteratureDOWCOM/dh_0032/0901b803800322b7.pdf?filepath=glycerine/pdfs/noreg/115-00667.pdf&fromPage=GetDoc.